Use of Microwave Dressing Fields to Enhance Rydberg Atom Interactions

by

Joseph A. Petrus

Presented to the University of Waterloo
in partial fulfillment of the
requirements for Physics 437A

January 19th 2007

Abstract

A microwave dressing field was used to induce resonant energy transfer in translationally cold Rydberg atoms. The ^{85}Rb Rydberg atoms were obtained by laser excitation of cold atoms in a magneto-optical trap. When the amplitude of a 1.356 GHz dressing field was scanned, the two-atom dipole-dipole process $43d_{5/2} + 43d_{5/2} \rightarrow 45p_{3/2} + 41f_{5/2,7/2}$ was enhanced due to the induced degeneracy of the initial and final states. The resulting spectrum had a series of resonant field amplitudes corresponding to different magnetic sublevels possible for the states involved. The scanned field amplitude was calibrated using microwave spectroscopy of the $43d_{5/2} - 41f$ transition under the influence of non-resonant dressing fields. The calibrated resonant field amplitudes agree well with ac Stark shift calculations performed using the Floquet approach. This method for enhancing interactions is complementary to dc electric field induced resonant energy transfer, but benefits from the ability to shift energy levels in either direction by choice in frequency.

Contents

List of Tables

List of Figures

1 Introduction

An atom with an electron in a highly excited, loosely bound state is known as a Rydberg atom. This highly excited configuration gives the atom a large transition dipole moment, making the atom very sensitive to electric fields [5]. In the present work, this property of Rydberg atoms is exploited to induced resonant energy transfer (RET) in cold Rb atoms via Stark shifts.

It is well known that dc electric fields can be used to enhance interactions between Rydberg atoms using the Stark effect [5, 10]. Here we show that not only can ac electric fields be used, but they can be used in situations where a dc electric field cannot.

1.1 Background

RET is a phenomenon that occurs when a pair of atoms can have the same total energy in two different state configurations. If this condition is satisfied then one atom may give its energy to the other and the two atoms involved rapidly transfer energy. For a generic set of states this can be written as:

$$A + A \rightarrow B + C. \tag{1}$$

In our case the process is driven by dipole-dipole interactions between the two atoms involved, but there are other possibilities. Fig. 1 illustrates this process.

RET will not occur naturally, therefore we must modify the energy levels of our atoms to be able to make the process resonant. The natural choice to modify Rydberg atom energy levels is an electric field because Rydberg atoms are extremely sensitive to electric fields [5]. The modification of energy levels by an electric field is called the Stark effect and will be discussed further in later sections. A schematic diagram indicating how the energy levels shift into resonance is shown in Fig. 2.

Depending on the states chosen for A, B and C the difference in total energy between the initial and final states can vary by a huge amount. The particular process being used in the experiments presented here is:

$$nd_{5/2} + nd_{5/2} \rightarrow (n+2)p_{3/2} + (n-2)f_{5/2,7/2}, \tag{2}$$

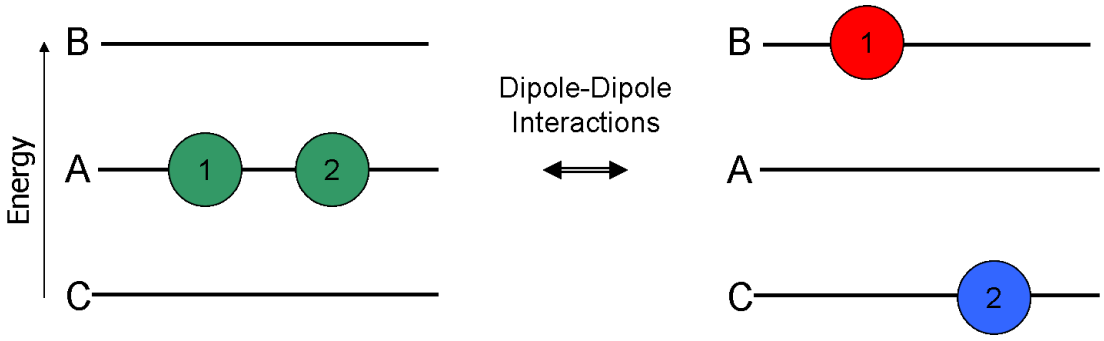

Figure 1: Illustration of RET. The key elements being that the total energy of the initial states is the same as that of the final states and that when the process occurs one atom is giving a specific amount of energy to another atom through dipole-dipole interactions.

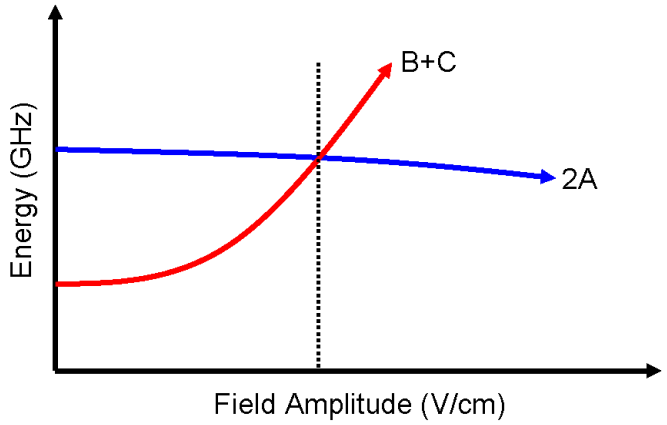

Figure 2: Schematic of RET. The zero field amplitude energy difference between 2A and B+C is called the mismatch. As the electric field amplitude is scanned, resonance is observed where the energy of 2A intersects the energy of B+C. Note: B+C may have a higher energy than 2A and the direction of the shift may be in either direction.

where n is the principal quantum number, d, p and f are the orbital angular momentum and 3/2, 5/2 , 7/2 are the total angular momentum. For this experiment to be feasible we must choose n such that the shift required to make the process resonant is minimal. To

determine n some simple calculations are performed.

Consider the energy of a Rydberg state, given by the following equation [5]:

$$E = \frac{-R_y}{(n-\delta_l)^2}, \tag{3}$$

where $R_y \approx 13.605$ eV is the Rydberg constant, n is the principal quantum number and δ_l is the quantum defect of the state of angular momentum l. The precise values of δ_l have been measured previously for many states [6] and so Rydberg atom energy levels can be easily calculated. Being able to calculate Rydberg atom energy levels with precision means that the mismatch of our process (Eq. 2) can be calculated with precision for various n. For convenience the quantum defects used for all calculations are included below [6].

Table 1: Quantum defect values of ^{85}Rb for s, p, d and f series

l	j	δ_0	δ_2
s	1/2	3.1311804	0.1784
p	1/2	2.6548849	0.2900
p	3/2	2.6416737	0.2950
d	3/2	1.34809171	-0.60286
d	5/2	1.34646572	-0.59600
f	5/2	0.0165192	-0.085
f	7/2	0.0165437	-0.086

The quantum defect of a nlj state is given by the following [5]:

$$\delta_{nlj} = \delta_0 + \frac{\delta_2}{(n-\delta_0)^2} + \frac{\delta_4}{(n-\delta_0)^4} + \dots \tag{4}$$

For our situation it is sufficient to include only the first two terms of the sum and use δ_0 and δ_2 from Table 1.

From Eq.'s 3 and 4 one can calculate the energy difference between the two initial states and two final states of Eq. 2) as a function of n. The result of such a calculation is shown in Fig. 3.

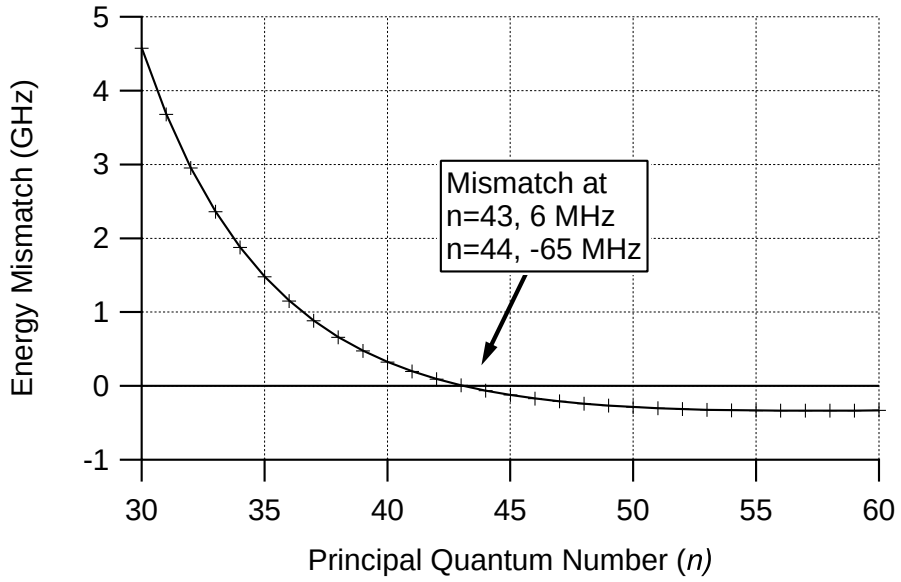

Figure 3: Calculation of the energy mismatch of $nd_{5/2} + nd_{5/2} \rightarrow (n+2)p_{3/2} + (n-2)f_{5/2,7/2}$ as a function of n.

From Fig. 3 one immediately notices that when $n = 43 \pm 1$ the energy mismatch is quite small. For $n = 43$ we have a mismatch of ≈ 6 MHz. A mismatch of this magnitude is quite possible to correct for (shift to 0 MHz) using either the dc or ac Stark effect. However, depending on n some interesting things occur - specifically, at $n = 43$ the dc Stark effect tunes the process out of resonance, while the ac Stark effect can tune it into resonance! To understand the origin of this phenomenon a closer look at the Stark effect is presented in later sections.

It is also interesting to keep in mind the various properties of Rydberg atoms and their dependence on n [5]. They are listed in Table 2.

Having found suitable n to use in Eq. 2, we will now take a closer look at how ac and dc electric fields are used to tune the process into resonance.

Table 2: Properties of Rydberg atoms

Property	n dependence
Binding energy	n^{-2}
Energy between adjacent n states	n^{-3}
Orbital radius	n^2
Geometric cross section	n^4
Dipole moment $\langle nd\|er\|nf\rangle$	n^2
Polarizability	n^7
Radiative lifetime	n^3
Fine-structure interval	n^{-3}

1.2 Stark Effect

When an atom is placed in an electric field the energy levels of this atom are temporarily shifted to a different energy. In general the magnitude and direction of this shift depends on the frequency and amplitude of the electric field being applied. This energy level shifting is called the Stark effect and is easily calculated for dc and ac electric fields.

In order to conceptually understand the results obtained for this experiment it is sufficient to consider the perturbative dc and ac Stark shift.

The dc Stark shift of a state $|\phi>$, in a dc electric field of magnitude ε_z in the z direction, is given by (see, for example, Ref. [11]):

$$\Delta E_\phi = \varepsilon_z^2 \sum_{m \neq \phi} \frac{|<\phi|\mu_z|m>|^2}{(E_\phi - E_m)}, \tag{5}$$

where E_m refers to the energy of state $|m>$ and μ_z is the electric dipole moment in the z direction and can be calculated using the techniques of Zimmerman *et al.* [13].

Similarly an equation of the ac Stark shift can be developed. The ac Stark shift of a state $|\phi>$, in an ac electric field oscillating at frequency ω, with amplitude ε_z in the z direction, is given by (see for example, Ref. [11]):

$$\Delta E_\phi = \frac{1}{2}\varepsilon_z^2 \sum_{m \neq \phi} \frac{(E_\phi - E_m)|<\phi|\mu_z|m>|^2}{(E_\phi - E_m)^2 - (\hbar\omega)^2} \tag{6}$$

A quick comparison of Eq.'s 5 and 6 reveals a few interest properties. First, Eq. 6 is equivalent to Eq. 5 when ω is set to 0 apart from a 1/2 factor due to time averaging the oscillating field. More importantly, in Eq. 6 we have an additional parameter in ω that can be used to alter the shift direction.

It is convenient to introduce the differential shift rate, $\kappa(\omega)$, of a particular state. It is defined by:

$$\Delta E_\phi = \kappa_\phi(\omega)\varepsilon_z^2, \tag{7}$$

where $\kappa(\omega)$ can be calculated from Eq.'s 5 and 6. The $\kappa(\omega)$ values for some illustrative states of Eq. 2 in a dc electric field and in ac electric fields detuned from the $(n-2)f_{7/2}$ to $(n-2)g_{9/2}$ transition by $\pm$150 MHz are shown in table 3.

Table 3: Differential shift rates for illustrative states ($m_j = 1/2$)

	κ in GHz/(V/cm)^2		
State	dc	ac, -150 MHz	ac, $+150$ MHz
$41f_{7/2}$	-2.0867	-4.8949	3.6986
$43d_{5/2}$	0.0061	0.0030	0.0030
$45p_{3/2}$	-0.0828	-0.0415	-0.0415
$42f_{7/2}$	-2.4708	-5.3801	4.0829
$44d_{5/2}$	0.0074	0.0037	0.0037
$46p_{3/2}$	-0.0973	-0.0488	-0.0488

Note: ac frequency relative to $41f_{7/2}$ - $41g_{9/2}$ (top three) and $42f_{7/2}$ - $42g_{9/2}$ (bottom three).

Table 3 indicates that the only states being shifted significantly are the f-states. It also shows that in a dc electric field the f-states will always be shifted to lower frequency, but for an ac electric field if the frequency is chosen above the $(n-2)f_{7/2}$ to $(n-2)g_{9/2}$ transition the f-state can be shifted to higher frequencies and vice versa. From Fig. 3 we know the mismatch for $n = 43$ to be 6 MHz. Since dc electric fields can only shift $(n-2)f_{7/2}$ to lower frequency (as seen in table 3), a dc electric field cannot be used to make Eq. 2 resonant for $n = 43$. However, since an ac electric field with a frequency of

1.356 GHz can shift $(n-2)f_{7/2}$ to higher frequencies we expect that such an electric field will be able to make Eq. 2 resonant and so our studies of ac electric field induced RET will be at a frequency of 1.356 GHz. On the other hand, when $n = 44$ the mismatch is -65 MHz so a dc electric field can be used to make Eq. 2 resonant.

Experiments confirming these predictions will be presented next. It should be noted that comparisons between experiment results and theory in subsequent sections use a more rigorous approach to calculate energy level shifts. The techniques of Zimmerman *et al.* [13] are used for dc Stark shifts and the Floquet approach is used for ac Stark shifts [12].

2 Experimental Techniques

The experimental investigation of Stark shift induced RET is not simple, but the procedure can be understood by taking a closer look at some of the more important aspects of the experiment. To begin, an overview of the experiment is provided, followed by a closer look at some of the more important topics. Details specific to a particular experiment are described in the relevant section.

The focal point of the entire experiment is our magneto-optical trap (MOT). The MOT provides a source of cold ($< 300\,\mu K$) Rb atoms. The MOT as well as some of its unique features have been described previously [2, 3]. Once we have a trap of Rb we use a frequency doubled Ti:Sapphire laser to excite the Rb to Rydberg states. From here a complex series of timing pulses allow us to expose the atoms to a variety of fields and subsequently detect the state distribution in the trap.

2.1 State Excitation and Analysis

In the process of cooling and trapping Rb, it is excited from its ground state of $5s$ to $5p_{3/2}$ by a diode laser. From here a frequency doubled Ti:Sapphire laser is used to excite the cold Rb atoms to specific Rydberg states. By tweaking the wavelength of the Ti:Sapphire appropriately we excite from $5p_{3/2}$ to $nd_{5/2}$, where for these particular experiments we are interested in $n = 43, 44$.

If the Rb energy levels are altered such that they satisfy the RET condition then some atoms in $nd_{5/2}$ will transition to either $(n+2)p_{3/2}$ or $(n-2)f_{5/2,7/2}$ through dipole-dipole interactions. The entire process is schematically shown in Fig. 4.

To do any sort of experiment using our Rydberg atoms we must be able to say something about the distribution of populated states in the trap. This is accomplished through a combination of selective field ionization, charged particle detection, boxcar integration and data collection. Each of these topics will now be elaborated on to illustrate how useful data is extracted from our experiments.

Rydberg atoms, being sensitive to electric fields, are easily ionized. The potential observed by a Rydberg electron both in the presence of an electric field and without is shown in Fig. 5. It is clear that as an electric field is applied the Rydberg states are

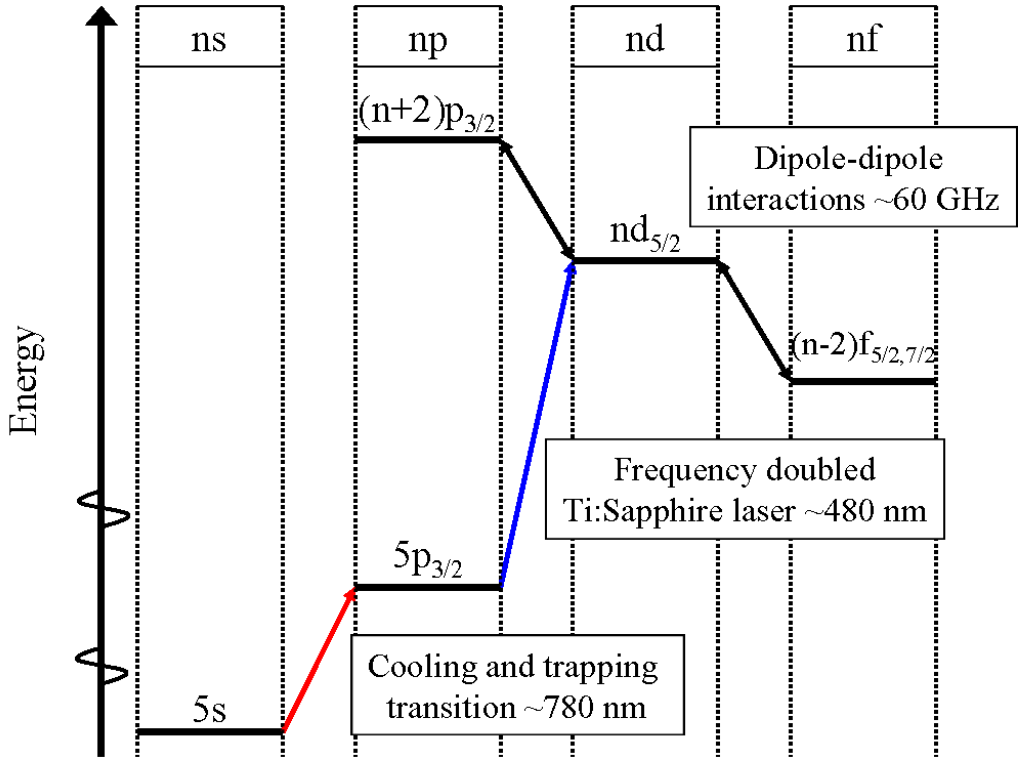

Figure 4: Schematic energy level diagram indicating the transitions involved.

easily ionized and this is exactly what selective field ionization (SFI) takes advantage of to determine state distributions.

A SFI pulse is coupled into the trap through two parallel plates located above and below the cloud of trapped Rb (see Fig. 6 for a schematic diagram of the trap). The pulse is essentially a large voltage ramp, increasing in time. As the voltage increases different states present in the trap are ionized at different times. When an atom is ionized the remainder of the SFI pulse forces the ion up to a microchannel plate (MCP) detector, producing a detectable current. Thus if a significant amount of some state is present in the trap a corresponding current is produced by the MCP detector. The resulting signal for a particular state has finite width in time (or equivalently SFI voltage). To gather the entire signal a set of boxcar integrators is used, one for each state involved ($nd_{5/2}$, $(n+2)p_{3/2}$

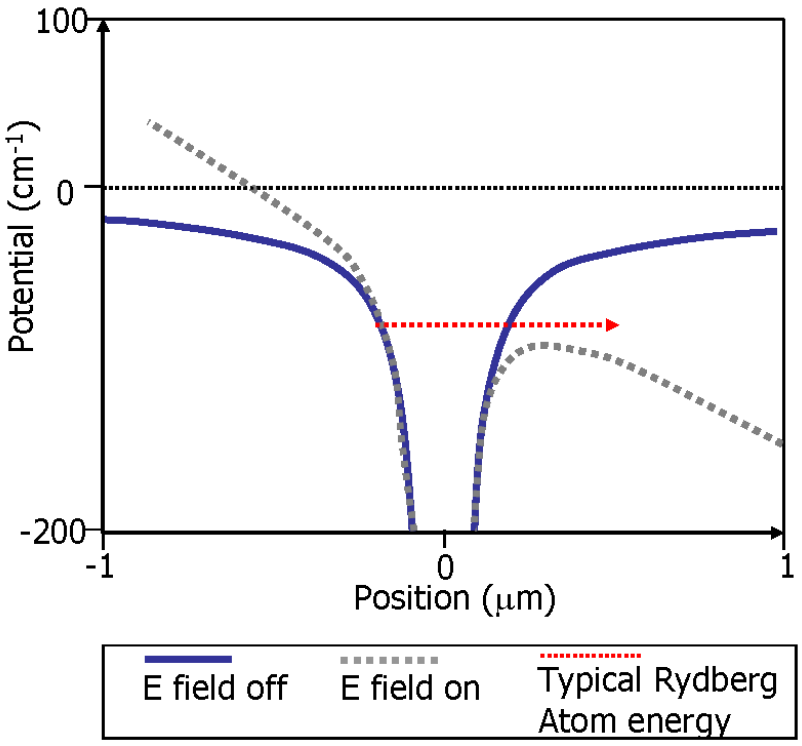

Figure 5: The solid line indicates the potential a Rydberg electron observes in the vicinity of the core without an external field. In this case the state shown would be bound. The dashed line indicates the potential a Rydberg electron observes in an electric field. If this electric field is strong enough the electron is quickly ionized.

and $(n-2)f_{5/2,7/2}$) as well as one for the "ion" signal. The signals captured by the boxcar integrators are sent to a LabView program through an analog to digital converter and we can now see how the state distribution changes if we repeat the experiment with a different electric field present.

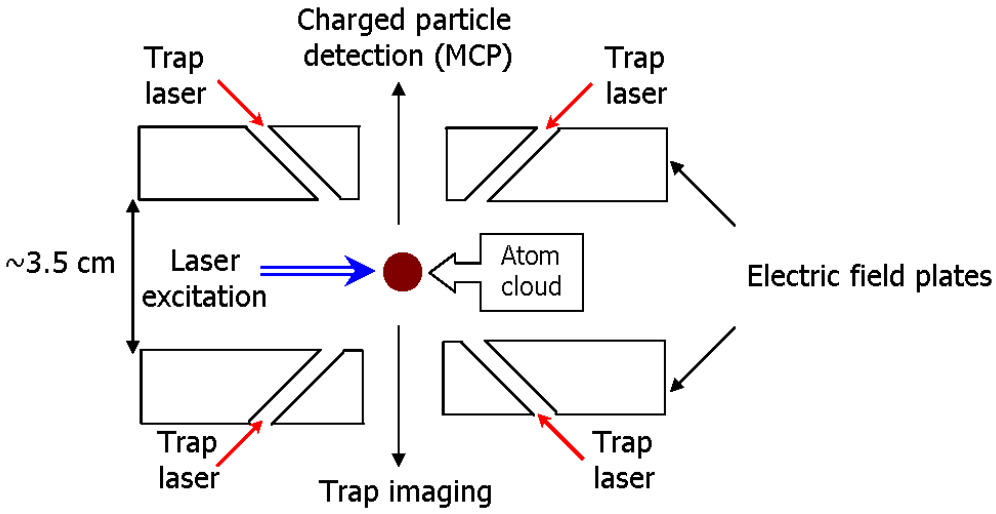

Figure 6: Schematic diagram of the electric field plates inside the vacuum chamber. The plates are used to couple ac and dc electric fields into the trap as well as for the SFI pulse.

3 DC Field Induced Resonant Energy Transfer

Dc electric field induced RET of $nd_{5/2}+nd_{5/2} \rightarrow (n+2)p_{3/2}+(n-2)f_{5/2,7/2}$ was investigated for $n = 44, 43$. As was mentioned in the introduction, we expect that when $n = 44$ we will see RET peaks, but when $n = 43$ we will not. Experimental details specific to this study are presented, followed by our results.

3.1 Experimental

To observe dc Stark shift induced RET we excite cold Rb atoms to Rydberg states as was described previously. Next a specific dc electric field is imposed on the atoms, which are then given 20 μs to interact. Finally a SFI pulse is used to determine the distribution of states present in the trap. This process is repeated at a rate of 10 Hz, for each repetition the dc electric field strength is increased slightly. The product of this procedure is state population versus field strength data. When Eq. 2 is off resonance the majority of the population is in the $nd_{5/2}$ state. As the electric field is increased, tuning the process into resonance, the population of $nd_{5/2}$ will decrease and simultaneously the population of $(n-2)f_{5/2,7/2}$ and $(n+2)p_{3/2}$ will increase. Thus if we plot the normalized population of $(n+2)p_{3/2}$ (or $(n-2)f_{5/2,7/2}$) versus the electric field strength we would have peaks indicating field strengths at which the process is resonant (see Fig. 2 for schematic). A simple illustration of the timing is shown in Fig. 7.

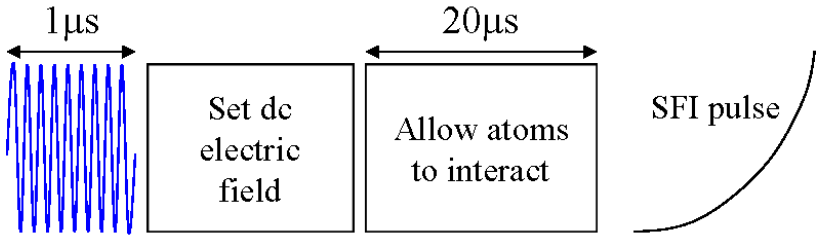

Figure 7: Schematic timing diagram for dc electric field induced RET. Shown is a 1 μs optical Rydberg state excitation pulse from the Ti:Sapphire, dc field strength setting, interaction waiting time of 20 μs and the SFI pulse. This sequence is repeated at 10 Hz.

Calibration of dc electric field strengths in our lab has been described and used previously (see Ref. [1]).

3.2 Results

To begin, we excited $44d_{5/2}$ and the population of $46p_{3/2}$ was collected as a function of field strength. The resulting data is plotted in Fig. 8.

In Fig. 8 we see that our calculations and experiment are in excellent agreement. The smaller peaks at high field strengths have not yet been discussed. They arise from high angular momentum states ($k = l > 5$) being tuned into resonance. Although this is a nice result, it is already known that dc electric fields can be used to induce RET. Things start to get interesting if we now look at $n = 43$.

Repeating the same procedure, only modifying the state we initially excited to $n = 43$ and the signal being collected to $45p_{3/2}$, the results are plotted in Fig. 9.

Here we only see peaks from the high angular momentum states ($l > 5$), Eq. 2 is tuned out of resonance as expected. This provides direct evidence that ac electric field induced RET is required under some circumstance.

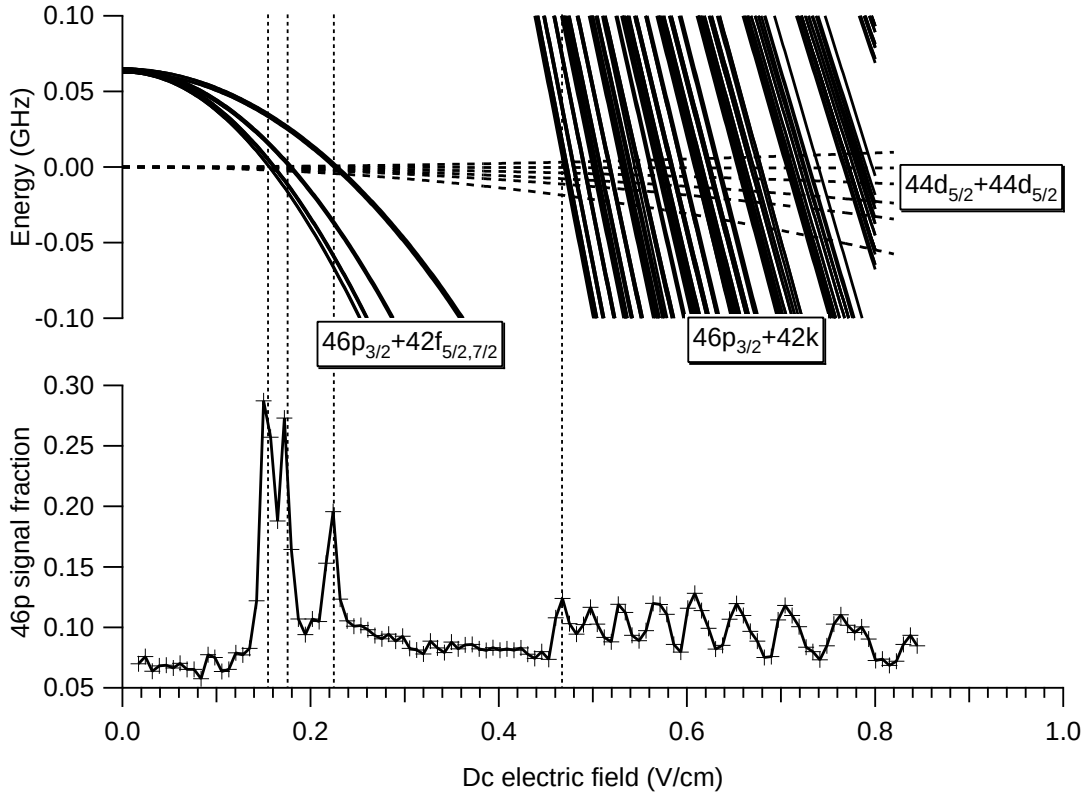

Figure 8: Comparison between calculation and experiment for dc electric field induced RET when $n = 44$. We expect to see RET peaks at field strengths where the energies of the initial and final states intersect. Note: Splitting is due to the different magnetic sublevels involved and energies are relative to two unperturbed $44d_{5/2}$ atoms.

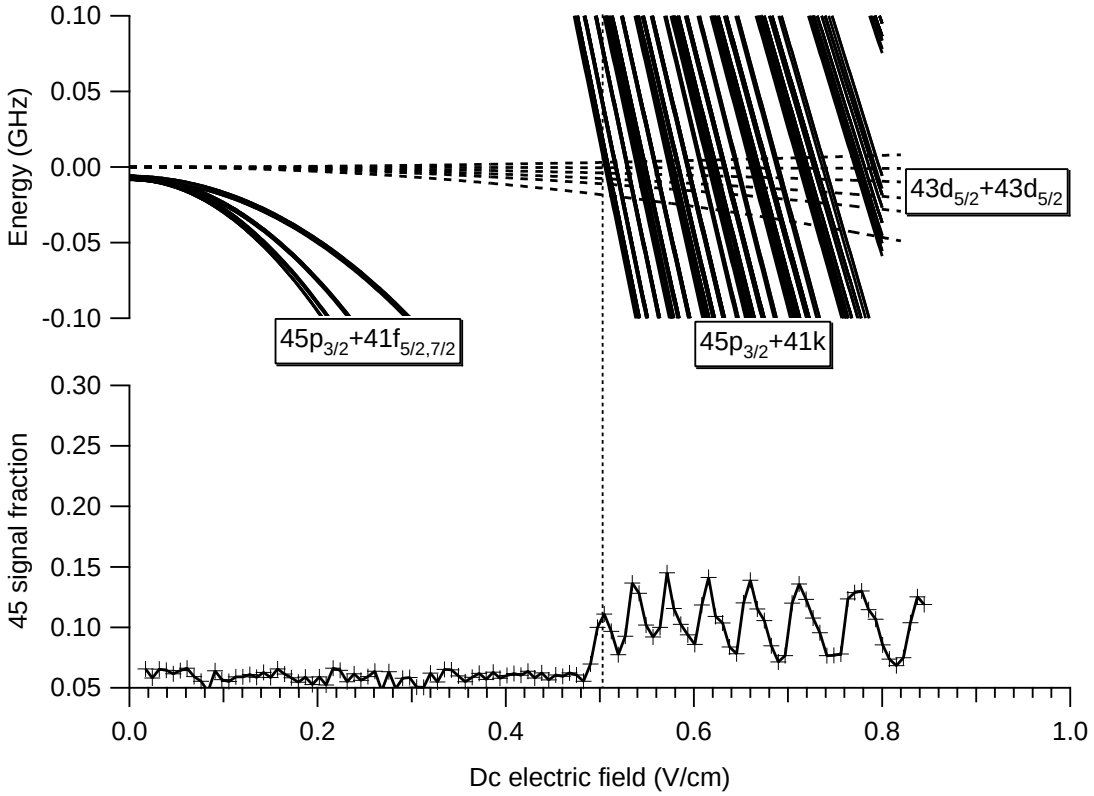

Figure 9: Comparison between calculation and experiment for dc electric field induced RET when $n = 43$. We expect to see RET peaks at field strengths where the energies of the initial and final states intersect. Note: Splitting is due to the different magnetic sublevels involved and energies are relative to two unperturbed $43d_{5/2}$ atoms.

4 AC Field Induced Resonant Energy Transfer

In the previous section it was shown that dc electric fields cannot always be used to Stark shift $nd_{5/2} + nd_{5/2} \rightarrow (n+2)p_{3/2} + (n-2)f_{5/2,7/2}$ into resonance. Based on the calculations presented earlier it is expected that we can use the ac Stark effect to tune it into resonance for $n = 43$. The experimental details specific to this experiment are summarized next, followed by the results.

4.1 Experimental

Similar to the dc electric field experiment, to observe ac Stark shift induced RET we excite cold Rb atoms to Rydberg states as was described previously. Next a 1.356 GHz ac electric field is imposed on the atoms at some field amplitude, which are then given 20 μs to interact. Finally a SFI pulse is used to determine the distribution of states present in the trap. This process is repeated at a rate of 10 Hz, for each repetition the ac electric field amplitude is increased slightly. The product of this procedure is state population versus field amplitude data. When Eq. 2 is off resonance the majority of the population is in the $nd_{5/2}$ state. As the electric field is increased, tuning the process into resonance, the population of $nd_{5/2}$ will decrease and simultaneously the population of $(n-2)f_{5/2,7/2}$ and $(n+2)p_{3/2}$ will increase. Thus if we plot the normalized population of $(n+2)p_{3/2}$ (or $(n-2)f_{5/2,7/2}$) versus the electric field amplitude we would have peaks indicating field strengths at which the process is resonant (see Fig. 2 for schematic). A simple illustration of the timing is shown in Fig. 10.

Calibration of ac electric field amplitudes is described in the appendix.

4.2 Results

$43d_{5/2}$ was excited and the population of $45p_{3/2}$ was collected as a function of dressing field amplitude (with the frequency of the field held constant at 1.356 GHz). The resulting data is plotted in Fig. 11.

In Fig. 11 we see many resonance peaks originating from the different magnetic sublevels of $41f_{5/2}$ and $41f_{7/2}$ and they seem to agree very well with what was predicted by

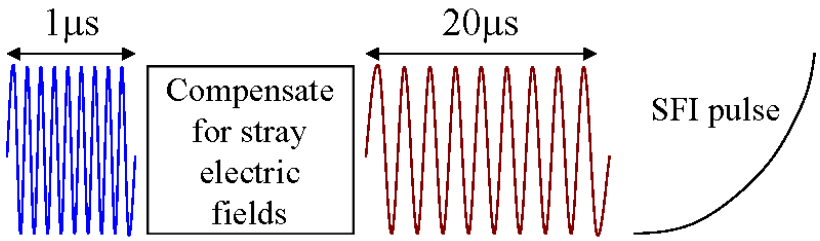

Figure 10: Schematic timing diagram for ac electric field induced RET. Shown is a 1μs optical Rydberg state excitation pulse from the Ti:Sapphire, dc field compensation, microwave dressing pulse of 20 μs and the SFI pulse. This sequence is repeated at 10 Hz.

Floquet calculations. Thus, we have shown that it is possible to use an ac electric field to Stark shift $nd_{5/2} + nd_{5/2} \rightarrow (n+2)p_{3/2} + (n-2)f_{5/2,7/2}$ into resonance under conditions where a dc electric field cannot.

4.3 Discussion

The results in the previous section provide conclusive evidence that it is possible to use an ac electric field to induce RET. However, to further confirm our results we repeated our measurements at various Rb densities. It was found that the signal scales linearly with density - a property of dipole-dipole interactions. We have also shown previously that it is possible to use high frequency microwave fields to induce RET, see Ref. [4].

Although the calibration method used gives very good agreement between our experiment and calculations it was assumed in the calibration process that we were only dealing with $m_j = 1/2$, which is not necessarily true. Further investigation is required to determine either why the calibration works as well as it does or if a different calibration technique is required.

The agreement of the calculations and experiments for the dc and ac electric field induced RET agree very well in terms of structure. The slight discrepancy in field strengths (amplitudes) is most likely due to the uncertainty in stray electric field compensation.

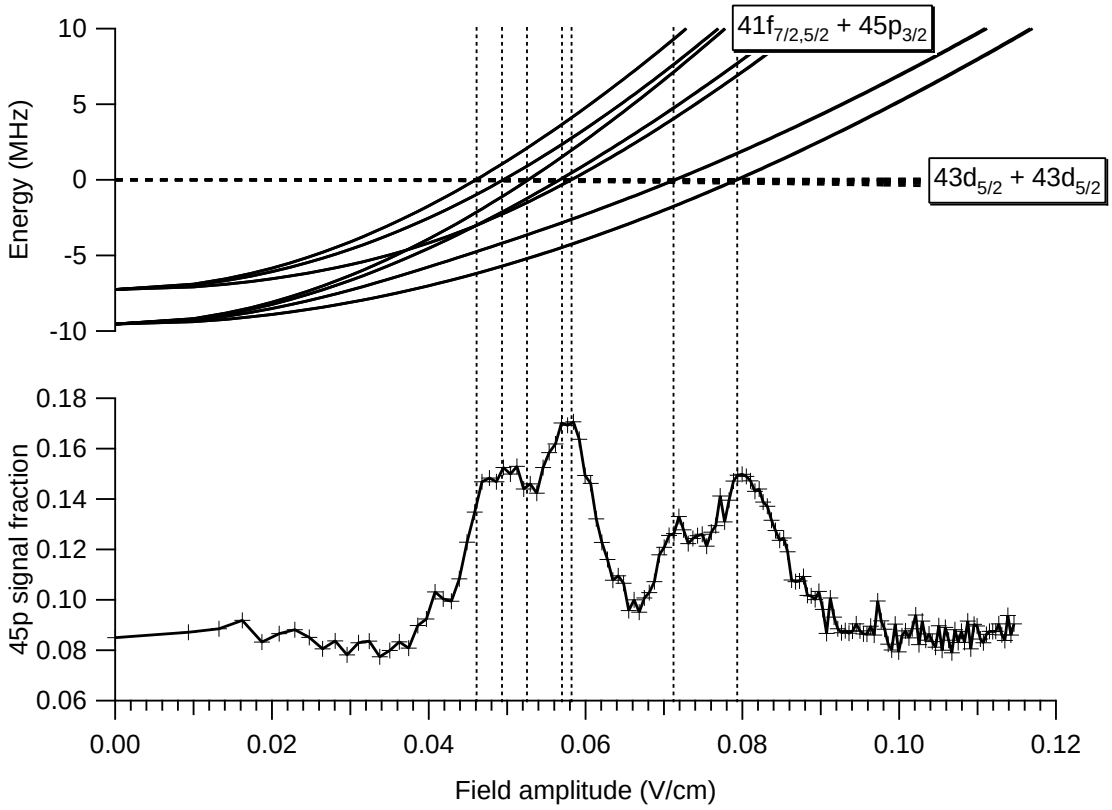

Figure 11: Comparison between calculation and experiment for ac electric field induced RET when $n = 43$. We expect to see RET peaks at field amplitudes where the energies of the initial (dashed line) and final states (solid line) intersect. The final states originating from lower energy are due to $41f_{7/2}$, the others are from $41f_{5/2}$. Note: Splitting is due to the different magnetic sublevels involved and energies are relative to two unperturbed $43d_{5/2}$ atoms. Also, the accumulation of data points at higher amplitudes is due to the field being scanned linear in power (rather than amplitude).

5 Conclusion

Ac electric field induced RET has been demonstrated. In addition it has been shown that an ac electric field can induce RET in situations where it is impossible to achieve using a dc electric field.

Being able to use an ac electric field to induce RET also has some technical advantages over its dc counterpart. For example, using an ac electric field would allow the dc electric field to be varied and ac electric fields can be quickly modulated.

RET has long been a topic of interest to atomic physicists and more recently it has been receiving attention due to its potential use in quantum information processing. For example, it has been proposed that dipole-dipole interactions between Rydberg atoms could be useful for quantum gates [8], or to encode qubits in clouds [9].

It has also been proposed that microwave dressing fields can be used to reduce the dc polarizability of Rydberg states [7]. This could be used to reduce the influence of dc electric field inhomogeneities on the dephasing of a Rydberg atom qubit and will likely be studied in future work.

Acknowledgements

It is with great pleasure that I acknowledge the assistance I have received from the Martin group. In particular I would like to thank Parisa Bohlouli-Zanjani and Kourosh Afrousheh for teaching me how to run the experiments, Jeff Carter and Owen Cherry for their coffee break support and discussions and last but not least Jim Martin for the countless hours of assistance in theory, experiment and everything else!

6 Appendix

6.1 Stark Map

A Stark map indicates the energy of many states as a function of dc electric field strength. Such a plot provides a useful overall picture of the relevant energy levels. Using the efficient methods developed by Zimmerman *et al.* [13] the Stark map of Rb was calculated around $n = 44$ and is included here for reference. See Fig. 12 and also the close up of the manifold ($42k$,$l > 5$) in Fig. 13.

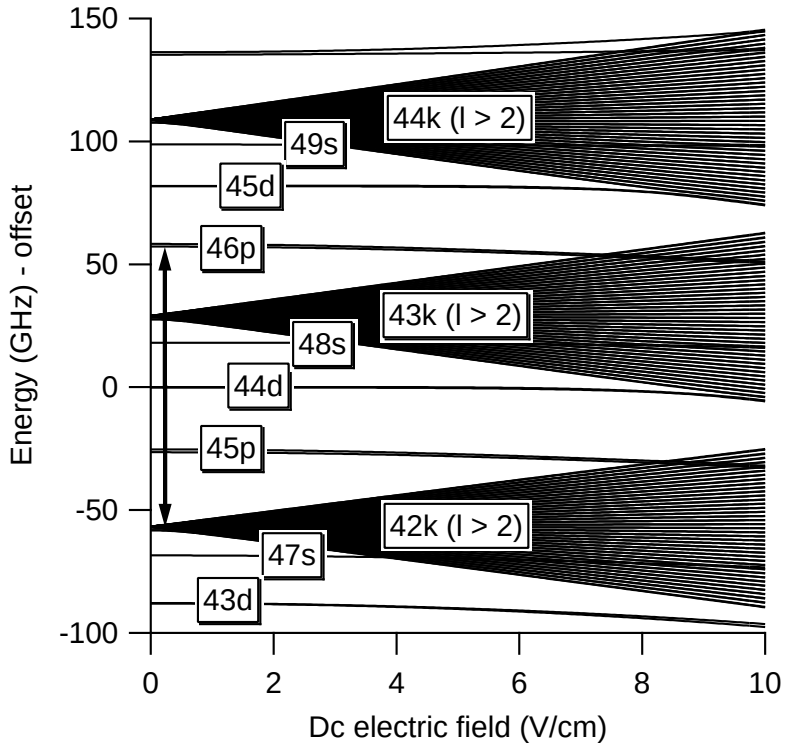

Figure 12: Calculation of the dc Stark map around $n = 44$. The arrows indicate the resonance of $44d_{5/2} + 44d_{5/2} \rightarrow 42f + 46p_{3/2}$ occurring for some field strength.

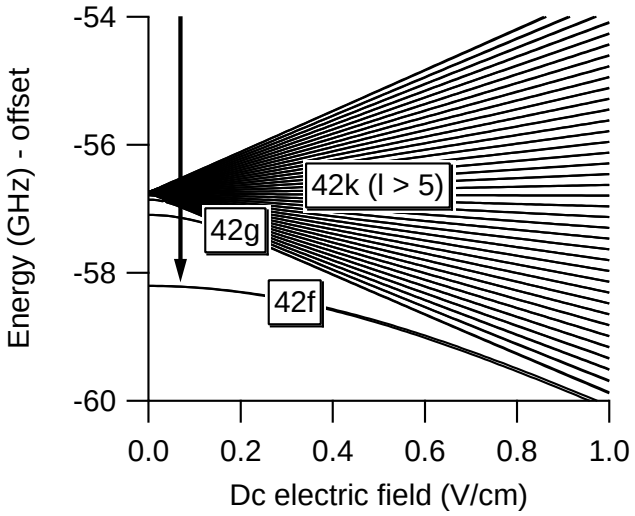

Figure 13: Calculation of the dc Stark map for states around $42f$. The figure indicates the strong quadratic shift of the f-state as well as the f-state being separated from the manifold ($42k$,$l > 5$).

6.2 AC Electric Field Calibration

While dc electric field strength calibrations have been done previously in our lab (See Ref. [1]), this is the first instance where an ac electric field amplitude calibration was required. The process used for calibration is described here for reference.

We require a procedure that allows us to relate the power setting on the synthesizer (P_{synth}) to the field amplitude as experienced by our trapped Rb (F_{trap}). To begin, it is useful to introduce γ as a calibration factor allowing us to calculate experimental shift from the differential shift rate, $\kappa(\omega)$, and P_{synth}. The equation relating these terms is:

$$\Delta E = \kappa(\omega)\gamma P_{synth}. \tag{8}$$

Taking an observed shift ΔE, the calculated $\kappa(\omega)$ and synthesizer power P_{synth}, γ can be calculated and used in the following relationship to convert synthesizer power (P_{synth}) in mW to a field amplitude (F_{trap}) in V/cm.

$$F_{trap} = \sqrt{\gamma P_{synth}} \tag{9}$$

Since the microwave dressing power is in dBm, it is useful to recall:

$$P_{mW} = 10^{[P_{dBm}/10]} \tag{10}$$

since it is sometimes easier to deal with mW.

6.2.1 Experimental

The experimental aspect is very similar to both of the other experiments. For the calibration we excite cold Rb atoms to $43d_{5/2}$. Using the timing shown in Fig. 14, the $43d_{5/2}$ to $41f_{5/2,7/2}$ transition frequency is measured by collecting the $41f$ signal as the frequency of a probe microwave is scanned (at constant power) first without a dressing field present. The procedure is then repeated with a 10 dBm (P_{synth}) dressing field. Taking the shift of this transition it is possible to calculate the calibration factor, γ, and consequently the calibrated field amplitude.

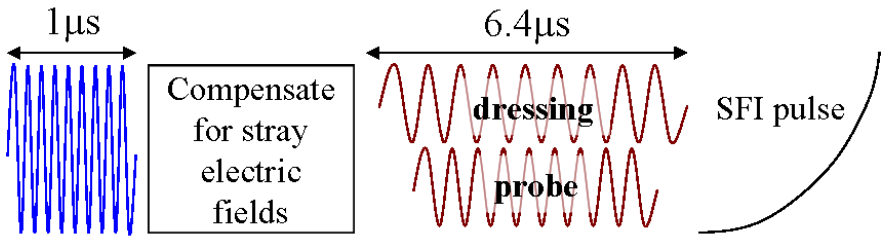

Figure 14: Schematic timing diagram for ac electric field calibration. Shown is a $1\,\mu$s optical Rydberg state excitation pulse from the Ti:Sapphire, dc field compensation, microwave dressing pulse of 6.4 μs, microwave probe pulse of 6 μs and the SFI pulse.

6.2.2 Results

With the dc electric field compensated as described previously, and no dressing field applied to the atoms a probe microwave (going through a frequency doubler) is scanned from 31.265 GHz to 31.271 GHz at low power. The resulting peaks are at 31.26866 GHz ±10 kHz and 31.26757 GHz ±10 kHz (found using a Gaussian fit) corresponding to $41f_{7/2}$ and $41f_{5/2}$

respectively. From equation 3 we expect these peaks at 31.2683 GHz and 31.2672 GHz, an acceptable difference given that the dc electric field uncertainty is ±30 mV/cm.

Next we apply a 10 dBm dressing field at our selected frequency of 1.356 GHz and measure the transition again. Under the influence of this dressing field the probe is scanned from 31.264 GHz to 31.271 GHz at low power. This time the peaks appear at 31.26709 GHz ±10 kHz and 31.26597 GHz ±10 kHz corresponding to $41f_{7/2}$ and $41f_{5/2}$ respectively. These peaks are shown in Fig. 15 along with the peaks observed without a dressing field present.

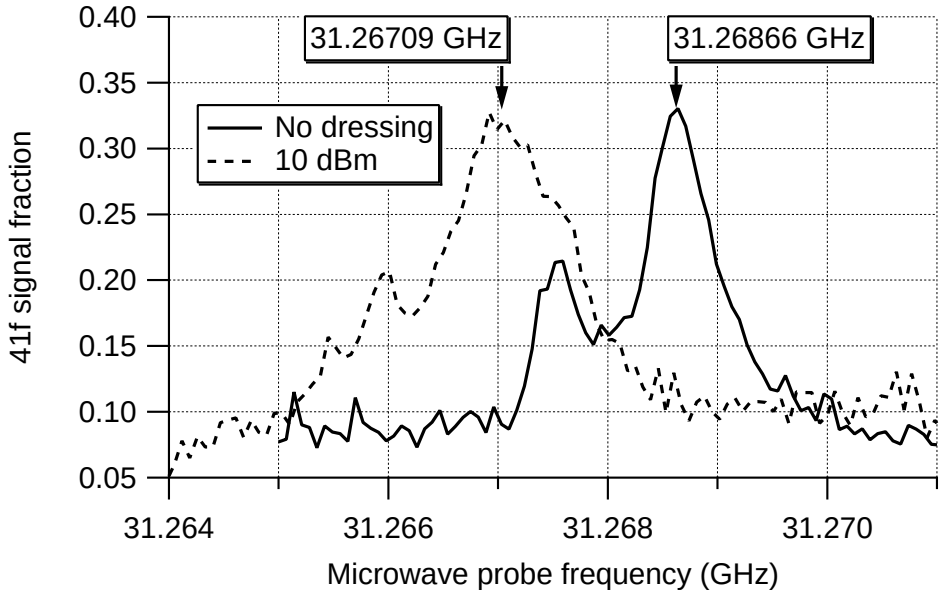

Figure 15: The solid line is the $43d_{5/2}$ - $41f$ transition driven by a low power probe microwave in the absence of a dressing field. The dashed line is the same transition now with a 10 dBm, 1.356 GHz dressing field. The difference between the peaks indicated can be used to calibrate the dressing field amplitude. Note: because a frequency doubler is used, frequencies shown here must be doubled.

Taking the difference between peak locations for $41f_{7/2}$ (doubling values to take care of the doubler's effect), we have a shift of 3.14 MHz ±15 kHz. Since the dressing frequency (ω) is constant for the above measurements we can calculate $\kappa(\omega)$ for $43d_{5/2}$ and $41f_{7/2}$

at $\omega = 1.356$ GHz assuming the only magnetic sublevel involved is $m_j = 1/2$. Taking the difference results in a differential shift rate for the transition equal to $-3.696\ \mathrm{GHz/(V/cm)^2}$. Recalling Eq. 8 we now have the following.

$$\Delta E = -3.696\gamma P$$

From our calibration spectra above we have a power and shift combination, allowing us to solve for the conversion factor, γ. Note: Eq. 10 implies 10 dBm = 10 mW.

$$\begin{aligned}\gamma &= \frac{\Delta E}{-3.696P} \\ &= \frac{0.00314\ \mathrm{GHz}}{-3.696\ \mathrm{GHz/(V/cm)^2} \times 10\ \mathrm{mW}} \\ &= 8.50 \times 10^{-5} \pm 4 \times 10^{-7} \frac{\mathrm{(V/cm)^2}}{\mathrm{mW}}\end{aligned}$$

Using γ, the field amplitude in V/cm being coupled into the trap can be easily calculated as follows.

$$F_{trap} = \sqrt{\gamma P_{synth}} \tag{11}$$

Where P_{synth} is expressed in mW and γ is calculated above. Equation 11 can now be used as a calibration for our ac Stark shift induced RET data.

References

[1] K. Afrousheh, P. Bohlouli-Zanjani, J. A. Petrus, and J. D. D. Martin. Determination of the ^{85}Rb ng-series quantum defect by electric-field-induced resonant energy transfer between cold Rydberg atoms. *Phys. Rev. A*, 74:062712, 2006.

[2] K. Afrousheh et al. Resonant electric dipole-dipole interactions between cold Rydberg atoms in a microwave field. *Phys. Rev. A*, 73:063403, 2006.

[3] P. Bohlouli-Zanjani, K. Afrousheh, and J. D. D. Martin. Optical transfer cavity stabilization using current-modulated injection-locked diode lasers. *Rev. Sci. Instrum.*, 77:093105, 2006.

[4] P. Bohlouli-Zanjani, J. A. Petrus, and J. D. D. Martin. arXiv, physics/0612233, 2006.

[5] T. F. Gallagher. *Rydberg Atoms*. Cambridge University Press, 1994.

[6] T. F. Gallagher, P. Pillet, M. P. Robinson, B. Laburthe-Tolra, and M. W. Noel. Back and forth between Rydberg atoms and ultracold plasmas. *J. Opt. Soc. Am. B*, 20:1091, 2003.

[7] P. Hyafil et al. Coherence-preserving trap architecture for long-term control of giant Rydberg atoms. *Phys. Rev. Lett.*, 93:103001, 2004.

[8] D. Jaksch, J. I. Cirac, P. Zoller, S. L. Rolston, R. Côté, and M. D. Lukin. Fast quantum gates for neutral atoms. *Phys. Rev. Lett.*, 85:2208, 2000.

[9] M. D. Lukin et al. Dipole blockade and quantum information processing in mesoscopic atomic ensembles. *Phys. Rev. Lett.*, 87:037901, 2001.

[10] K. A. Safinya, J. F. Delpech, F. Gounand, W. Sandner, and T. F. Gallagher. Resonant Rydberg-atom-Rydberg-atom collisions. *Phys. Rev. Lett.*, 47:405, 1981.

[11] I. I. Sobel'man. *Introduction to the Theory of Atomic Spectra*. Pergamon Press, 1972.

[12] W. van de Water et al. Microwave multiphoton and excitation of helium Rydberg atoms. *Phys. Rev. A*, 42:572–591, 1990.

[13] M. L Zimmerman, M. G. Littman, M. M. Kash, and D. Kleppner. Stark structure of the Rydberg states of alkali metal atoms. *Phys. Rev. A*, 20:2251, 1979.